Preparation and Characterization of Hybrid Membranes based on Nafion®
using Partially Sulfonated Inorganic Fillers

F. J. Fernandez-Carretero[1], E. Riande[2], C. del Río[2], F. Sanchez[2], J. L. Acosta[2] and V. Compan[1,*]

[1] Departamento de Termodinámica Aplicada. ETSII. Universidad Politécnica de Valencia. 46020, Valencia, Spain.
[2] Instituto de Ciencia y Tecnología de Polímeros (CSIC), 28006, Madrid, Spain.

Abstract: *This work reports the preparation and characterization of inorganic hybrid membranes cast from solutions of perflouorinated sulfocationic ionomers (Nafion® 117) containing 10 wt % dispersed inorganic fillers. Silica gel, SBA-15 and sepiolite, all of them partially functionalized with sulfonic acid groups, were used as fillers. Fillers slightly reduce the water uptake without altering the ion-exchange capacity of the membrane composites. FTIR and DMTA analysis techniques suggest that filler-polymer matrix interactions are stronger with sepiolite than with the other fillers. The fillers used enhance the mechanical properties of the membranes, but they negatively affect the thermal stability of the composites. The permeability coefficient of oxygen in Nafion® and Nafion®-sepolite membranes is similar, and it is slightly lower in the others. The conductivity of the hybrid membranes equilibrated with water, measured at 80° C by impedance spectroscopy, is 4.0, 6.0 and 6.3 S/m for the hybrid membranes containing functionalized Silica gel, SBA-15 and Sepiolite fillers, respectively, somewhat lower than that found for the Nafion® 117 membrane, 5.9 S/m, measured in the same conditions.*

Keywords: Hybrid Nafion® membranes; Sepiolite, Proton conductivity, Oxygen Permeability, PEMFC.

1. INTRODUCTION

The synthesis of cation-exchange membranes that combine low protonic resistance and good mechanical properties is nowadays a flourishing field of research. The interest in membranes arises in part from the potential use of these materials as electrolytes in low temperature fuel cells [1]. Operating at moderately high temperature in order to decrease platinum catalyst poisoning by effect of traces of carbon monoxide in hydrogen fuel, provokes water evaporation. Membrane dryness causes a drop of conductivity thus becoming one of the most significant barriers to run with polyelectrolytes in fuel cells. As a result, high temperature operating conditions requires a significant increase of the pressure of the humidified fuel to keep a suitable amount of water in the membranes that facilitates protons transport from the anode to the cathode, otherwise the protonic conductivity drops several orders of magnitude. Moreover, drag of water by the traveling protons, called electro-osmotic effect, also contributes to the membrane dryness, though this effect is in part compensated by back diffusion of water produced in the cathode. As a consequence, different alternatives are being investigated to maintain high values of conductivity in dehydrated environments [2-3]. On the other hand, membranes used as electrolytes in fuel cells should exhibit high mechanical and thermal stability in hot oxidative atmospheres.

Perfluorinated ionomers are up to date the best materials to develop cation-exchange membranes that meet the requirements of high protonic conductivity and good mechanical and thermal stability at temperatures lying in the range 50 - 90ºC [4-6]. However the need of working at higher temperatures requires developing membranes that maintain high conductivity in dehydrated environments. This is a key issue in the progress of the development of low temperature fuel cells for practical purpose [2-3]. Other drawbacks of perfluorinated membranes are their high permeability to reformers such as methanol, high cost and environmental effects.

In principle, fillers may improve water retention in polyelectrolytes under low relative humidity conditions thus preserving the protonic conductivity of membranes at relatively high temperatures [7]. Also fillers may hinder reformers permeability across membranes. The information at hand suggests that the incorporation of hygroscopic particles such as SiO_2, ZrO_2, TiO_2, zirconium phosphate and sulfophenyl phosphonates into the hydrophilic domains of membranes leads to some improvement in the perform-
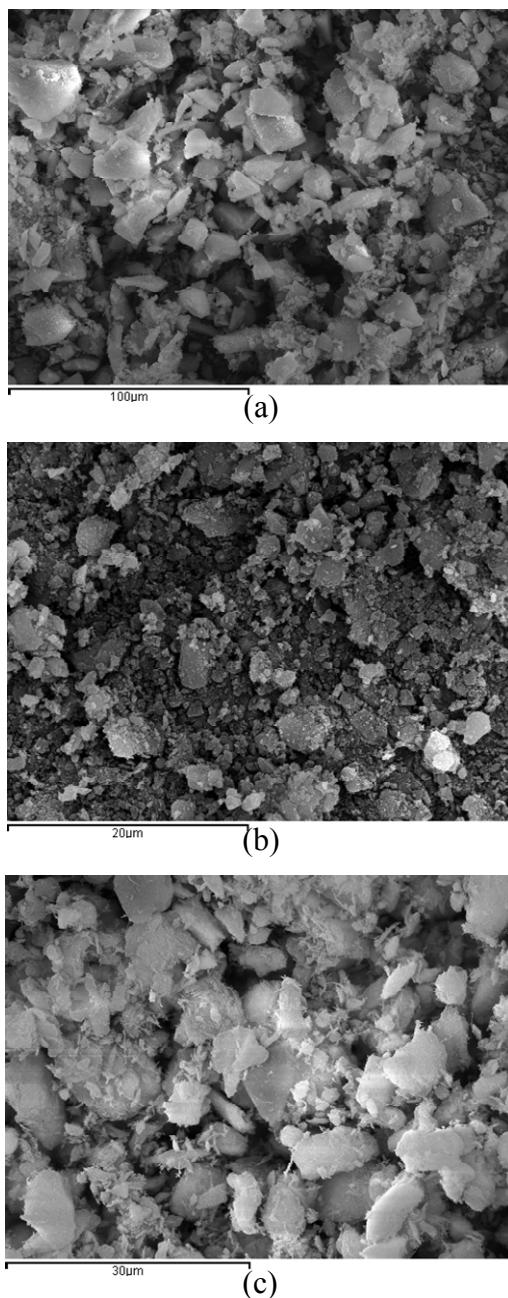
(a)

(b)

(c)

Figure 1. SEM micrographs of sulfonated: a) Silica gel (SIL), b) SBA-15 and c) Sepiolite (SEP).

Table 1. Ionic Exchange Capacity of fillers and particle size

Sample	IEC (mmol g⁻¹)	Particle size (mm)
SIL	0.072	17
SBA	0.34	3
SEP	0.23	7

ance of acidic membranes such as Nafion [8-21]. Pursuing this line of research, this work reports the preparation of inorganic-organic hybrid membranes by incorporating phenyl-sulfonated inorganic materials into Nafion® 117 ionomers. Polymer matrix-filler interactions were analyzed by FTIR spectroscopy and the

effect of fillers on thermal stability of the composites was studied by both thermogravimetry and differential scanning calorimetry. Attention is paid to the effect of the fillers on the conductivity, mechanical properties and thermal stability of the acidic Nafion® membranes. The membranes were characterized by measuring water uptake, ion-exchange capacity and conductivity. Also, the effect of the fillers on oxygen transport in the membranes equilibrated with water was investigated. The results obtained show the improvements and drawbacks caused by the introduction of fillers in Nafion membranes.

2. EXPERIMENTAL PART

2.1. Fillers

Silica gel, SBA-15 and Sepiolite were used as starting materials. Fillers functionalization was carried out by reaction of the hydroxyl groups of the inorganic particles with phenyl-tri-ethoxisilane. Sulfonation of the phenyl groups was carried out with sulphuric anhydride at room temperature. Synthesis and characterization of the sulfonated fillers involving size and thermal properties were reported elsewhere [22]. The acronyms used for phenyl sulfonated silica gel, SBA-15 and sepiolite were, respectively, SIL, SBA and SEP. The average size of the sulfonated particle fillers was obtained from the SEM micrographs shown in Figure 1, and the pertinent results together with the sulfonation degree of the fillers are collected in Table 1.

2.2. Preparation of hybrid membranes

Hybrid membranes based on Nafion® containing 10% of solid fillers were prepared by adding the required amount of sulfonated filler of interest to a commercial Nafion®117 solution under stirring. After 6 h of ultrasonic dispersion, the apparently homogeneous substrate was cast on a smooth Petri dish, and solvent evaporation from the apparently homogeneous dispersion proceeded at 70ºC for 2h, and then at room temperature until apparent total solvent elimination. Finally the membranes were dried under vacuum for 2h [23].

2.3. Water uptake and ionic exchange capacity

The fillers ion exchange capacity was determined both by elementary analysis and titration. A 0.01M NaOH solution was prepared and titrated with 0.01M potassium hydrogen phthalate.0.5 g of the filler were suspended in 20 ml of 0.1M KCl at least 24h. Suspension was filtered and liberated protons were titrated with the 0.01M NaOH.

Weighed dry membranes were immersed in distilled deionized water overnight. The membranes were removed from water, gently blotted between filter paper to eliminate surface water and weighed. This operation was repeated three times. Water uptake was calculated by means of the expression

$$\text{Water uptake} = \frac{\text{weight of wet membrane - weight of dry membrane}}{\text{weight of dry membrane}} \times 100 \quad (1)$$

The membranes ion-exchange capacity (IEC) was obtained by immersing the membranes in the acid form in 1 M NaCl solution. The protons liberated in the exchange reaction R-SO$_3$H + Na$^+$ → R- SO$_3$Na + H$^+$ were titrated with a 0.01 M NaOH solution. The IEC was obtained as

Preparation and Characterization of Hybrid Membranes based on Nafion® using Partially Sulfonated Inorganic Fillers
/ J. New Mat. Electrochem. Systems

85

$$IEC = \frac{0.01V}{m} \qquad (2)$$

where V and m are, respectively, the volume in *liters* of NaOH solution spent in the titration of the protons released by m Kg of dry membrane. IEC is usually given in Equiv/Kg of dry membrane.

2.4. Surface analysis

Surface analysis of the fillers was done by means of isothermal N_2 adsorption at 77K A Micrometrics Tristar 3000 was employed for this purpose. Specific area was calculated using BET isothermal over a relative pressure range between 0.03 and 0.3 and assuming a cross section of adsorbed nitrogen of 0.162 nm^2.

2.5. Chemical and thermal characterization

Thermal analysis was carried out by differential scanning calorimetry using a DSC TAQ10, at a heating rate of 10ºC/min. Two scans from -80ºC to 300ºC were run for each sample.

The thermal stability of the membranes was determined by thermogravimetry, with a TA TGA Q500 apparatus. The experiments were carried out under nitrogen atmosphere, in the temperature range 50-800ºC, at a heating rate of 10ºC/min.

2.6. FTIR analysis

IR spectroscopy were used to check polymer matrix- fillers interactions. The spectra were obtained using a JASCO, FT/IR- 6200 with microscope IRT-300 IRTRON, and a NIR-FT-Raman Perkin-Elmer Spectrum 2000 apparatus equipped with a diode pumped Nd:YAG laser PSU.

2.7. DTMA analysis

Dynamic thermal mechanical analysis (DTMA) measurements were performed with a TA DMA Q800 experimental device operating in the film tension mode. Isochrones at 0.3, 1, 3, 10 and 30 Hz were obtained at a heating rate of 2ºC/min in the temperature window -140º - 250ºC. Immediately before starting the experiments, the samples were dried during 48h, at 90ºC, to assure total water elimination.

2.8. Oxygen permeability in the membranes equilibrated with water

Oxygen permeation measurements were performed using a Clark-type electrode fitted for the electrochemical determination of oxygen transmissibility in wet hydrogels. The amount of oxygen permeating across the swollen membranes equilibrated with water was computed from the measurement of the electric current generated by reduction of oxygen at the cathode of a modified polarographic electrode (Rehder Development Co., Castro Valley, CA). In this experimental device, the gold cathode of area (14.24±0.13) ´ 10^{-2} cm^2 is kept at - 0.75 V with respect to the silver anode coupled to a Model 201T O_2 Permeometer (Createch, Albany, CA). The silver anode is positioned concentrically to the cathode, and both electrodes are separated by an epoxy resin, forming a spherical cap. The measurements were carried out at 25º C.

The permeability coefficient of oxygen in the membranes at equilibrium with water was measured with electrochemical methods described by Aiba et al. [24], modified for the determination of the oxygen transmissibility and permeability coefficients of contact lenses and hydrogels using the following configuration: water saturated with air at 1 barômembraneômeshçelectrodes. Oxygen transmissibility in the membranes was measured according Compañ et al. [25], following the ISO/DIS 9913 and 9913-1 standards procedure [26].

In steady state conditions, the flux of oxygen across the membranes is given by Fick's first law

$$J = -P\frac{p_2 - p_1}{L} \cong P\frac{p_1}{L} \qquad (3)$$

where P is the permeability coefficient of oxygen in the membrane, L is the thickness of the membrane and p_2 and p_1 are, respectively, the pressures at the sides of the membranes in contact with the electrodes and with water saturated with air. Owing to the nearly instantaneous reduction of oxygen in the electrodes, p_2 is negligible. The intensity of current, I, generated by the reduction of the flow of oxygen permeating through the membrane is given by

$$I = 4FAP\frac{p_1}{L} \qquad (4)$$

where F (=96,480 C/equiv) is Faraday's constant and A is the permeation area of the membrane in contact with the cathode. The ratio P/L is commonly known as transmissibility coefficient. The oxygen transmissibility is calculated from the steady electrical current, I_{st}, using the following equation.

$$\frac{P}{L} = \frac{I_{st}}{4FAp_1} \qquad (5)$$

The measurements were carried out without previous treatment of the membranes, following the procedure described elsewhere [27]. The electrodes were first moistened with a drop of distilled water before adjusting the wet membrane on the cathode. The vertical hollow cylinder was adjusted to the membrane, after inserting a wet piece of mesh between the cathode and the membrane. Finally, a small quantity of distilled water (0.5 cm^3) was introduced by the opening of the cylinder so that all system was exposed to environmental atmosphere. The current starts at a high level in all cases, due to the saturation of oxygen in the membrane-cathode compartment, but decreases rapidly reaching steady state conditions after 7-8 minutes. The values of the current intensity in steady-state conditions were used to determine, respectively, the transmisibility and permeability coefficients of oxygen of the membranes.

2.9. Conductivity measurements

Impedance spectroscopy measurements in the frequency range 10^{-2} - 10^7 Hz and temperature window 25 – 80ºC were conducted on the membranes, using voltage amplitudes of 0.1V. The membranes previously equilibrated with water were placed between two gold electrodes coupled to a Novocontrol Broadband Dielectric Spectrometer (Hundsangen, Germany) integrated by a SR 830 lock-in amplifier with an Alpha dielectric interface. During the measurements the membranes were kept equilibrated with water at the temperatures of interest [28], controlled by nitrogen jet (QUATRO from Novocontrol) with a temperature error of ≈ 0.1 K for every single sweep in frequency.

Proton conductivity was obtained from Nyquist and Bode dia-

grams fitting the response to an analogical electric circuit consisting of a resistance that accounts for the protonic resistance in series with one or more circuits made up of a resistance that accounts for the polarization resistance of the membrane in parallel with a constant phase element accounting for interfacial phenomena in the membrane-electrodes interface. The proton resistance of the membranes was taken from the Bode plot as the value of the modulus of the complex impedance at which the phase angle reaches a maximum, close to 0, in the high frequencies region [29].

3. RESULTS AND DISCUSSION

3.1. Fillers characterization

From the % of sulphur results obtained from the fillers elementary analysis, ion Exchange capacity was calculated by using:

$$IEC = \frac{1000 \cdot \%S}{100 \cdot 32} \tag{6}$$

The results obtained are shown in table 2. This table show elementary analysis results non sulfonated and sulfonated samples respectively. SEP01 and SEP02 samples correspond to two sepio-

Table 2. Elementary analysis results of non sulfonated fillers and sulfonated fillers.

Sample	non sulfonated fillers		sulfonated fillers		
	C (%)	H (%)	C(%)	H (%)	S (%)
SBA (synthesis)	13.17	2.27	11.54	2.43	1.07
SBA (grafting)	5.55	1.71	5.08	1.93	0
SIL	7.89	1.09	6.84	1.18	0.20
SEP01	17.81	2.28	5.33	1.57	0.82
SEP02	7.58	1.68	2.73	1.66	0.73

Table 3. Results comparison of ionic exchange capacity obtained by elementary analysis with the obtained by titration.

Sample	Sulfonation (h)	IEC (EA) (mmol/g)	IEC (Titration) (mmol/g)
SBA-15 (synthesis)	45	0.33	0.34
SBA-15 (grafting)	48	0	0.15
SIL	60	0.0625	0.072
SEP01	65	0.26	0.23
SEP02	65	0.23	0.039

Table 4. Fillers carbon losses obtained from the elementary analysis results.

Sample	C (before sulfonation) (mmol/g)	C (after sulfonation) (mmol/g)	DC (%)
SBA-15 (synthesis)	1.83	1.60	12.6
SBA-15 (grafting)	0.77	0.70	9.1
SIL	1.02	0.88	14.0
SEP01	2.47	0.74	70.0
SEP02	1.05	0.10	90.5

Table 5. Results of isothermal adsorption of N_2 at 77K.

Sample	Single Point Surface (m²/g)	P/P⁰ (SPS)	BET surface (m²/g)	v_m (cm³/g STP)
Sílica gel	462.9	0.297	476.5	109.5
SIL	440.3	0.296	460.3	105.7
SBA-15	691.8	0.302	711.2	163.4
SBA	770.1	0.310	787.7	180.9
Sepiolite	135.4	0.302	139.8	32.1
SEP	201.6	0.305	210.1	48.3

lite samples prepared by varying the moiety grafting reaction time. It was of 17h in SEP01 sample and 5h in SEP02 sample. We observed that increasing reaction time; more organic moieties are incorporated to the filler. However, after sulfonation, most of the organic is lost and %S is similar in the two samples.

From the results of the elementary analysis and the acid-bases titration, ion exchange capacity is obtained in mol/g as it has been described in the experimental part. The results are shown in table 3, indicating too, the sample sulfonation time. In general, the number of incorporated acid groups to solids is low. A greater reaction temperature or greater times would be a possible solution to this problem.

The percentage of sulfonic groups is higher in the SBA-15 prepared by synthesis than in grafted SBA-15. Grafting procedure is not suitable for the preparation of sulfonated SBA-15.

Carbon present in the samples before and alter sulfonation determined by means of the elementary analysis can be useful to check if the organic moiety is lost after sulfonation. In table 4 we can observe the obtained results for the fillers carbon losses. Second and third column show the %C before and after sulfonation and the fourth column show the difference. From these results is clear that in sepiolite, most of the organic moiety is lost after sulfonation, maybe for an aggressive treatment and maybe because moiety was not correctly grafted to the Sepiolite.

3.2. Isothermal N_2 adsorption

BET model was employed for fitting the experimental data of isothermal N_2 adsorption. The results of surface analysis are shown in the table 5. We observe that in the silica gel samples, functionalization reduces the specific surface. In the phenyl sulfonated SBA-15, we observe a higher specific surface than in non functionalized SBA-15. This is explained by the presence of surfactant not eliminated after the synthesis that is removed after during the functionalization and the post sulfonation. Functionalized Sepiolite has a greater surface than non functionalized Sepiolite. This is due to the previous acid treatment during the filler functionalization. This treatment with HCl eliminates Mg liberating attached silanol groups and increasing Sepiolite area [30]. This treatment causes the octahedric layer breaks and the silica formation [31]. Can be observed that, in the functionalized fillers, SBA-15 has the greater specific surface followed by the silica and the Sepiolite.

3.3. TGA analysis

Thermograms showing the thermal degradation of the hybrid membranes as well as the loss weight peaks are presented as a function of temperature in Figure 2. For comparative purposes, the curve describing the thermal stability for the pristine Nafion® membrane is also shown. The loss of mass observed in the vicinity of 100ºC corresponds to traces of water, whereas the mass loss in the temperature range 270-360ºC is caused by degradation of sulfonic groups. The rather sharp loss weight taking place in the range 400 – 550ºC, proceeds from degradation of the polymer backbone. It is worth noting that the degradation curves show that Nafion® membranes are more stable than the hybrid ones. A similar behavior was reported by Di Noto et al. [32] who observed that 9% in weight of silica causes a significant decrease in the thermal stability of composite Nafion® membranes. Taking as reference the temperature at which 5% of decomposition takes place (see last column in Table
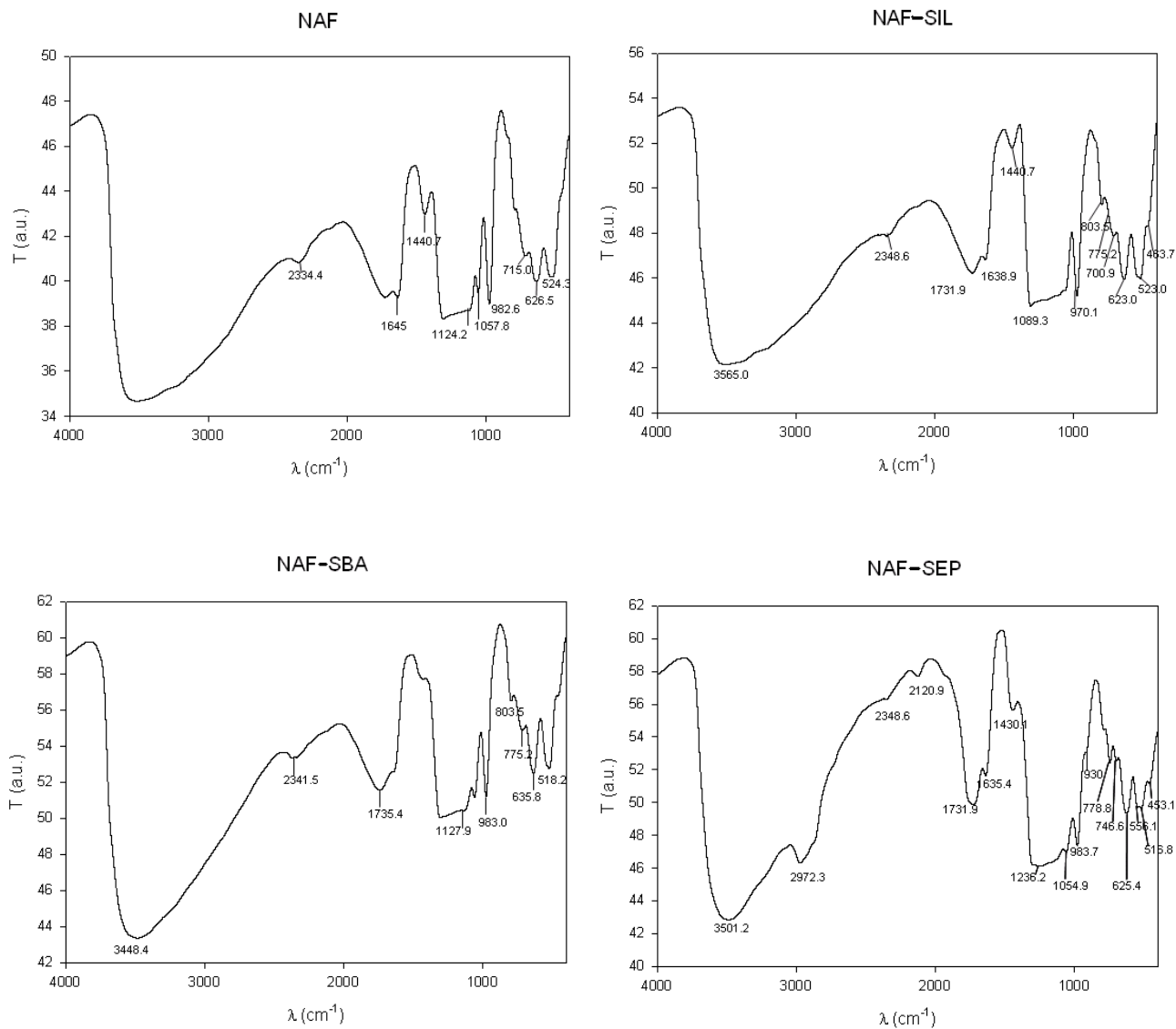
Preparation and Characterization of Hybrid Membranes based on Nafion® using Partially Sulfonated Inorganic Fillers
/ J. New Mat. Electrochem. Systems

87

Figure 3. FTIR spectra of Nafion® and Nafion® hybrid membranes.

Table 6. Percentages of loss of water, ionic groups and polymer weight in pristine Nafion® and Nafion hybrid membranes obtained from TGA experiments. The residual mass of the membranes and the temperature at which 5% of polymer is lost in TGA experiments are also indicated.

Sample	Water weight (%)	SO_3H weight (%)	Polymer weight (%)	Residue weight (%)	$T_{5\%}$ (ºC)
Nafion®	3.2	8.9	86.6	1.2	407
NAF-SIL	3.1	9.7	85.1	2.0	401
NAF-SBA	2.7	9.1	77.0	10.5	402
NAF-SEP	2.9	8.9	77.0	10.0	384

6), the thermal stability of the membranes follows the trends: T(Nafion®) > T(NAF-SBA) > T(NAF-SIL) > T(NAF-SEP).

The percentages of loss of weight of water, sulfonic acid groups and polymer backbone for hybrid and pristine Nafion® membranes

are shown, respectively, in the second, third and fourth columns of Table 6, whereas the percentage of the residues is given in the fifth column of the table. It can be seen that the sulfonic acid loss percentage is similar for all the samples despite the fact that hybrid membranes have 10% less of polymer than pure Nafion® ones. This result agrees with the IEC results, which are similar for all the membranes.

The thermal degradation curves exhibit more than one stage owing to complicated mechanisms involving several parallel and/or series reactions [33-35]. The final residue in the samples containing SBA-15 and Sepiolite is approximately 10% of the weight of the respective membranes, similar to the percentage of solid fillers. In the hybrid membranes containing silica gel as filler, the final residue was lower, presumably due to the reaction of SiO_2 with HF produced in the degradation of the polymer backbone via the reaction

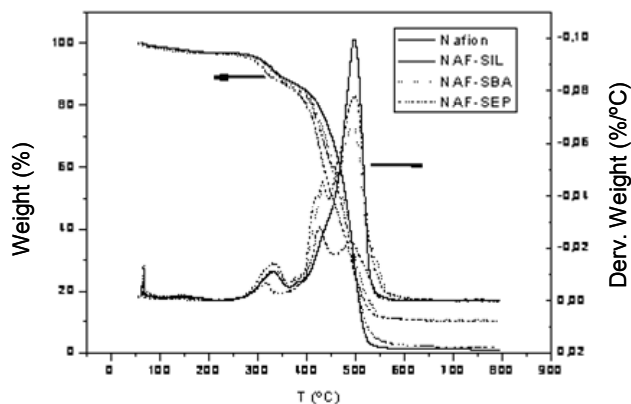Figure 2. TGA curves for Nafion® and Nafion® hybrid membranes. Mass loss as a function of temperature (continuous line) and first derivative of the mass loss (dash line).
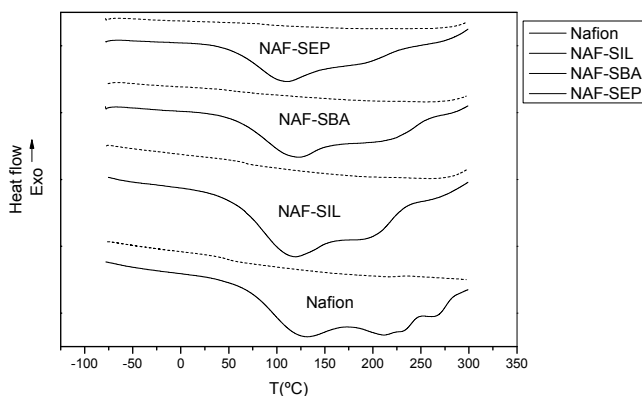

Figure 4. DSC results for the membranes. Continuous and dash lines represent, respectively, the first and second scans.

$$SiO_2 + 4HF \rightarrow SiF_4 + 2H_2O \qquad (7)$$

3.4. FTIR analysis

The characteristic bands of Nafion® in the FTIR spectra, shown in Figure 3, have higher intensity than the silicate bands. In the literature, stretching vibration of the Si-O-Si angle usually appears in the range 1090-1010 cm^{-1} [36]. In our samples, this band is overlapped with the high intensity SO$_3$H bands [37] giving rise to a saturation signal that extends to near 1200 cm^{-1}. Two bands, not detected in Nafion®, are observed in the NAF-SIL sample. One of the bands associated with the out-of-plane deformation vibration of the di-substituted phenyl moiety appears at 775.22 cm^{-1}. This band evidences the presence of sulfonated phenyl groups grafted to the fillers. Another band, at 463.71 cm^{-1}, is assigned to the Si-O-Si bond. The spectrum of the NAF-SBA membrane is similar to that of Nafion® except for the appearance of a band at 775.22 cm^{-1} corresponding to the di-substituted phenyl ring. The fact that the spectrum of the NAF-SEP membrane is better resolved than the spectra of the other composite membranes, suggests that the interactions between Nafion® and Sepiolite are more favourable than between
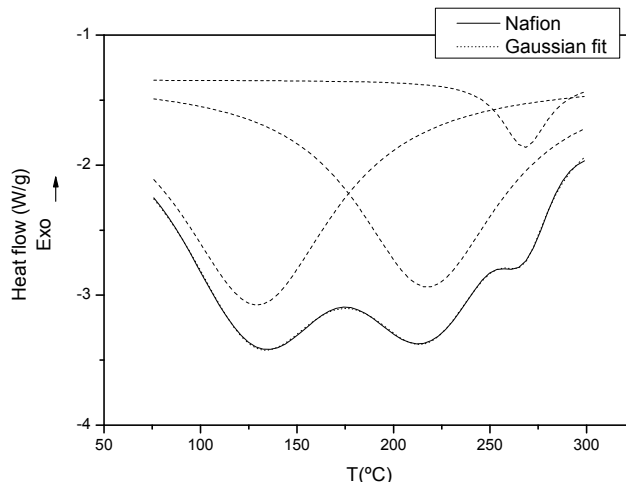

Figure 5. Gaussian fit for the curve of the first DSC scan of the Nafion® membrane.

this polymer and both SBA-15 and silica gel.

The band between 2800 and 3600 cm^{-1} corresponding to water is better defined in the hybrid membranes than in the Nafion® sample. A second band appearing at 2972.29 cm^{-1} is assigned to the stretching vibration of the C-H bond of the phenyl groups grafted to the Sepiolite. The band at 930 cm^{-1}, observed in the spectra of hybrid membranes, can be assigned to the stretching vibration of the Si-O bond of the Si-OH group. The band appearing at 453.1 cm^{-1} is also assigned to the Si-O bond.

3.5. DSC analysis

DSC curves showing the thermal behavior of the membranes in the temperature range [-80-300]ºC are presented in Figure 4. Continuous and dash lines correspond, respectively, to the first and second scans. Based on the results of the second scan, it is not possible to detect any transition in both pristine Nafion® and hybrid Nafion® membranes. Transitions which are seen in the first scan and absent on the subsequent heating, are attributed to residual water present in the membranes. It is also possible that the heat capacity for Nafion® and hybrid composites below and above the glass transition temperature is rather close, precluding the possibility that transitions are detected by DSC in dry membranes.

DSC curves corresponding to the first scan present three endothermic peaks labeled in increasing order of temperature I, II, III, the position of which depends on the membranes composition. The overlapped endothermic peaks in the first scan were deconvoluted using Gaussian functions. Figure 5 shows the Gaussian fit for the Nafion® membrane whereas the temperatures associated with the peaks for hybrid and Nafon membranes are given in Table 7. The peaks can tentatively be explained by assuming that membrane-traces of water structures are developed in the membranes. Thus the first peak (I) is presumably related to phase transitions at the ionic clusters brought about by traces of water. The presence of fillers in the membranes shifts this region to lower temperatures presumably due to disruption of the natural packing of the ionic clusters caused by the fillers [38]. The second peak (II) is related to the fusion of microcrystalline regions [39] whose formation is fa-
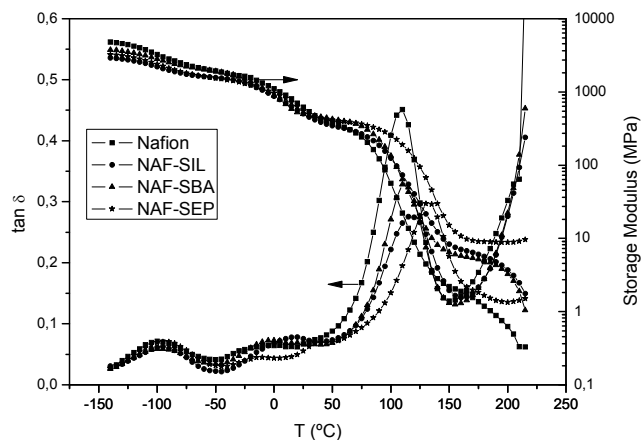
Figure 6. Storage modulus and loss tan d as a function of temperature, at 1 Hz, for the membranes indicated in the inset.

voured by the presence of traces of water. The fact that the location of this peak seems to be insensitive to the fillers suggests formation of microcrystalline domains in the membranes not hindered by the fillers. Finally the third peak (III) arises from the total disruption of ionic clusters whose formation was probably favoured by traces of water. Development of this latter peak presumably is the first step to degradation of the ionic groups attached to both Nafion® and the sulfonated inorganic particles. As occurs in TGA experiments, NAF-SEP and NAF membranes exhibit, respectively, the lower and higher temperatures at which the third peak is centred.

3.6. DMA analysis

The data of DMA analysis were collected at the rate of 2º C/min and frequency of 1 Hz, in an inert atmosphere of nitrogen. The temperature dependence of the storage modulus and tan δ are shown in Figure 6. Three decreasing steps are detected in the storage modulus, which become three peaks in the loss tan d isochrones of Figure 6. The origin of the three relaxation processes appearing in the isochrones of Nafion® have been reported elsewhere [38-40]. In brief, the relaxation centred at -100ºC, named γ relaxation, is followed by a weak process, called b absorption, located in the vicinity of 0º C. At temperatures slightly higher than 100ºC, an ostensible glass-rubber relaxation or a absorption, arising from segmental motion of Nafion® chains backbone, appears.

The γ relaxation, which is centered at the temperature at which this process appears in pure PTFE [33], is believed to be produced by hindered rotations of a very small number of segments [32]. Therefore the g relaxation is not affected by the fillers. The β process seems to arise from motions of the side chains of Nafion®. Since the ionic groups in Nafion® are attached to the side chains, the absorption is sensitive to the fillers that form part of the ionic clusters in the membranes. There is some controversy regarding the glass transition temperature of Nafion® 117. For example it has been suggested that the g relaxation is related to Tg [42], whereas some authors assume that the β process corresponds to the glass-rubber transition [43]. However, most authors believe that the glass transition temperature is associated with the ostensible relaxation centered in the vicinity of 110º C [32, 40-43]. In support of

this interpretation is the sharp drop occurring in the storage modulus taking place at this temperature. Yeo Eisenberg [44] have shown that the exchange of protons by sodium ions dramatically shifts both the β and a processes to higher temperature; for example, these shifts are, respectively, from 20 and 110º C to 22º C and 150º C. Therefore, the microstructure of ionic clusters that restrict the molecular motions of the backbone of the chains is strongly affected by the nature of the counterions. It seems that clusters containing protons keeps more loosely tight the chains than other counterions and hence both relaxations for the membranes in the acidic form appear at relatively low temperatures.

Values of the temperatures at which the relaxation processes are centered are collected, at 1 Hz, in Table 8. As indicated above, the storage modulus in the α relaxation undergoes a sharp and rather large decrease for Nafion® membranes. The drop of the modulus in the hybrid membranes is lower than in the pristine membrane because the fillers-polymer interactions decrease chains mobility. In turn, the decrease of the storage modulus in the glass-rubber relaxation is lower for the NAF-SEP membrane than for the other two hybrid membranes. The same occurs with ultimate mechanical properties [45-46]. Moreover, owing to the reduction of chains mobility caused by the fillers, the a relaxation produced by segmental motions of the perfluorinated chains is shifted to higher temperatures. It is worth noting that stronger Nafion®-Sepiolite interactions detected by FTIR are responsible for the higher T_a of the membranes.

Regarding to the β relaxation, there is no definite correlation between the location of this process and the nature of the fillers. This relaxation is influenced by the presence of traces of water in the sample, in such a way that the process is shifted to lower temperatures as the water content increases [40, 47]. This relaxation could be attributed to motions of the side groups. With the exception of the NAF-SIL sample, the β process for Nafion® and the hybrid membranes appear at similar temperature in the spectra. The fact that the relaxation in the NAF-SIL membrane is shifted to higher temperature suggests that either favorable polymer-filler interactions hinder the molecular motions of the side chains that produce the β process or the water content is lower than in the other membranes. The first cause seems unlikely because the loss of water at 100ºC is higher for Nafion and NAF-SIL membranes than for the other membranes (see Table 6). Therefore traces of water seem to be easier eliminated in the NAF-SIL than in both NAF-SBA and NAF-SEP membranes and, as a result, the β relaxation appears at higher temperature [46].

The γ relaxation is associated to local molecular motions in the hydrophobic regions of the polymer. The fact that the number of segments of the chains intervening in the development of the absorption is small explains that the γ relaxation is insensitive to the fillers.

Table 8. Temperatures associated with the peaks of the relaxation processes

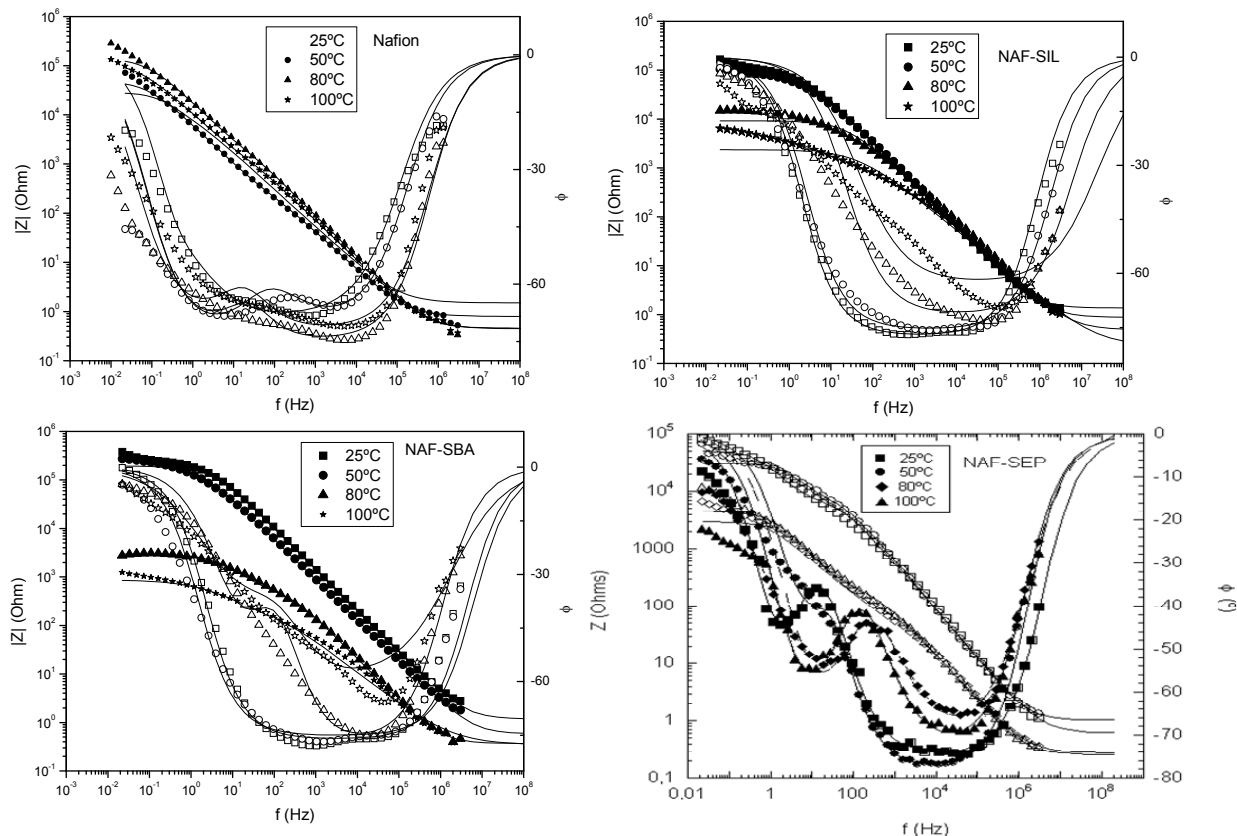|	T_α (ºC)	T_β (ºC)	T_γ (ºC)
Nafion®	109	-3	-102
NAF-SIL	116	16	-96
NAF-SBA	111	-2	-98
NAF-SEP	132	-9	-92

Figure 7. Bode plots for NAF, NAF-SIL, NAF-SBA and NAF-SEP membranes, equilibrated with water, at 25, 50, 80 and 100 ºC. The filled and open symbols represent, the modulus of the impedance and phase angle, respectively. The lines shown the fitting of the Bode diagram obtained from the analogic circuit of figure 8 to the experimental results.

Table 9. Values of the oxygen tansmissibility (P/L), and permeability, P, coefficients for Nafion® and hybrid membranes, at 25ºC.

Sample	Thickness (mm)	I_{est} (mA)	Transmissibility (Barrer/mm))	P (Barrer)
Nafion 117	180±5	2.35±0.3	6.2±0.7	11.1±1.6
NAF+SIL	65±2	5.70±0.4	15.0±1.0	9.8±0.8
NAF+SBA	160±5	2.45±0.3	6.3±0.8	10.1±0.7
NAF+SEP	100±4	4.3±0.4	11.3±1.0	11.3±0.4

Table 10. Water uptake and ion-exchange capacity (IEC) for Nafion® and hybrid membranes

Sample	Water uptake (%)	IEC (mmol H⁺/g dry membrane)	mol water/mol SO₃H⁻
Nafion®	36.6	1.04	19.6
NAF-SIL	24.1	1.11	12.1
NAF -SBA	31.7	0.99	17.7
NAF -SEP	22.3	0.90	13.7

3.7. Oxygen permeability across the membranes equilibrated with water

The oxygen transmissibility measured following the procedure described before in section 2.7. is an apparent value, because it corresponds to the system formed by the membrane, the wet piece of mesh and the small layer of distilled water containing a drop of borax, covering the cathode, which controls the pH. Consequently, the determination of the true permeability of the membrane requires measuring the apparent oxygen transmissibility of wet piece of mesh and water layer first, and then the total transmissibility for the system membrane+ wet piece of mesh + water layer. Taking into account that in the configuration water saturated with air (p_1 = 155 mmHg) çmembraneçpiece of mesh+water÷cathode, the drop of oxygen pressure can be expressed as $\Delta p_t = p_1 = \Delta p_m + \Delta p_{mesh+wt}$, eq 5 leads to

$$\left(\frac{L}{P}\right)_t = \left(\frac{L}{P}\right)_m + \left(\frac{L}{P}\right)_{mesh+wt} \tag{8}$$

or,

$$\left(\frac{1}{I}\right)_t = \left(\frac{1}{I}\right)_m + \left(\frac{1}{I}\right)_{mesh+wt} \tag{9}$$

From the two independent measurements of I_t and $I_{mesh+wt}$ the true value of I_m, and hence the transmissibility and permeability coefficients of the membrane are obtained. The values obtained for P are collected in Table 9. It can be seen that the permeability coefficient of oxygen follows the trends P(Nafion®) ≅ P(NAF-SEP) > (NAF-SAB > P(NAF-SIL). Accordingly, most of the fillers used in

Preparation and Characterization of Hybrid Membranes based on Nafion® using Partially Sulfonated Inorganic Fillers / J. New Mat. Electrochem. Systems
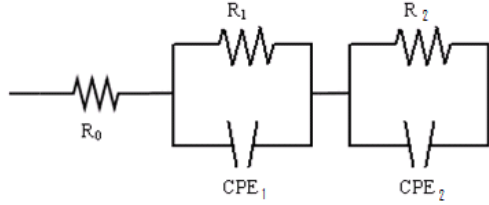
91

Figure 8. Equivalent electric circuit of the acidic membranes to an alternating electric force field, in a wide frequency window in the impedance measurements.

this study decrease oxygen crossover in the membranes indicating good compatibility between the fillers and the swollen polymer matrix.

3.8. Water uptake, ionic exchange capacity and conductivity

Values of the water uptake and ion-exchange capacity (IEC), collected in the second and third columns of Table 10, indicate that the substitution of 10% of polymer by fillers causes a reduction in the water uptake of the composite membranes. Moreover, despite the fact that the fillers were sulfonated, its low sulfonation index contributes to a slight decrease of the ionic exchange capacity of the hybrid membranes. As a result, fillers decrease the moles of water per mol of ionic groups.

Figures 7 show Bode plots corresponding to the Nafion® and the hybrid membranes equilibrated with water in the temperature range 25 – 100º C. The curves $|Z^*|$ *vs f* for the pristine Nafion membrane show that the modulus of the complex impedance decreases with increasing frequency until a plateau is reached in the high frequency region. As for the phase angle, $f = [\tan^{-1}(Z''/Z')]$, where Z' and Z'' are the real and imaginary components of Z^*, respectively, increases with frequency reaching a maximum. However, in the case of the composite membranes neither the plateau in the $|Z^*|$ *vs f* curves nor a maximum in the f *vs f* plots are reached at high frequency, in the frequency window used in the measure-

ments. To circumvent this problem, the circuit shown in Figure 8 containing two constant phase elements with admittances $Y^*_1 = Y_{01}\left(j\omega\tau_1\right)^{n_1}$ and $Y^*_2 = Y_{02}\left(j\omega\tau_1\right)^{n_2}$ was used to model the frequency dependence of both the complex impedance and the angle phase f. The impedance of the circuit can be written as

$$Z^* = R_0 + \sum_{i=1}^{2} \frac{R_i}{1 + R_i Y_{0i}\left(j\omega\tau_i\right)^{n_i}} \tag{11}$$

where $0 < n_i \leq 1$. Hence, the real and imaginary components of the complex impedance are given by

$$Z' = R_0 + \sum_{i=1}^{2} \frac{R_i\left[1 + Y_{0i} R_i\left(\omega\tau_i\right)^{n_i}\right]\cos\frac{n_i\pi}{2}}{1 + Y_{0i} R_i^2\left(\omega\tau_i\right)^{2n_i} + 2Y_{0i} R_i\left(\omega\tau_i\right)^{n_i}\cos\frac{n_i\pi}{2}}$$

$$Z'' = \sum_{i=1}^{2} \frac{Y_{0i} R_i^2\left(\omega\tau_i\right)^{n_i}\sin\frac{n_i\pi}{2}}{1 + Y_{0i} R_i^2\left(\omega\tau_i\right)^{2n_i} + 2Y_{0i} R_i\left(\omega\tau_i\right)^{n_i}\cos\frac{n_i\pi}{2}} \tag{12}$$

The analogical circuit used whose impedance is given by eq (11) fits fairly well the experimental data thus allowing the determination of the values of the complex impedance modulus at the plateau. Illustrative fitting plots for both the modulus of the impedance and the phase angle for pristine Nafion® membrane and Nafion® hybrid membranes containing 10% of fillers are shown as a function of frequency, at different temperatures, in Figure 7. The values of the parameters defining the analogical circuit of figure 8 that fits the results of Figure 7 are collected in Table 11. It can be seen that both the characteristic relaxation time and the resistance of the membrane to proton transport, R_0, decrease with increasing temperature, whereas the values of n_i that measure the departure of the polarization processes from Debye behaviour lie in the range 0.7 – 0.9. Similar behaviour is observed for the evolution of these parameters with temperature for the other membranes.

The proton conductivity was obtained from R_0 by

Table 11. Values of the parameters obtained from fits of analogical circuit show in figure 11 with the experimental results of Bode diagram show in figure 10.

		R_0 (Ohm)	R_1 (Ohm)	τ_1 (s)	n_1	R_2 (Ohm)	τ_2 (s)	n_2	l(μm)
NAFION	25	1.49	5230	9.12E-07	0.72	23500	8,47E-06	0.87	212
	50	0.79	113	6.81E-07	0.74	49000	3,15E-06	0.81	212
	80	0.46	432	5.32E-07	0.90	144000	8,39E-07	8,0.81	212
	100	0.45	454	3.12E-07	0.84	119000	8,04E-07	0.78	212
NAF-SIL	25	1.36	95900	4.26E-07	0.86	-	-	-	152
	50	0.88	74000	9.82E-08	0.84	-	-	-	152
	80	0.49	9260	7.03E-08	0.79	-	-	-	152
	100	0.45	2370	5.11E-08	0.70	-	-	-	152
NAF-SBA	25	1.18	2520	7.66E-07	0.81	244000	2,90E-08	0.85	173
	50	0.58	1500	6.66E-07	0.78	195000	1,78E-08	0.84	173
	80	0.37	1840	4.07E-07	0.61	2630	1,30E-08	0.78	173
	100	0.35	1140	3.57E-08	0.51	810	9,99E-09	0.59	173
NAF-SEP	25	1.02	25700	3.78E-07	0.84	551000	1,39E-07	0.87	125
	50	0.62	6220	8.44E-08	0.83	44700	5,83E-08	0.87	125
	80	0.26	150	7.79E-08	0.81	4390	2,97E-08	0.82	125
	100	0.27	90	6.85E-09	0.77	2860	1,24E-08	0.81	125

$$\sigma = \frac{l}{R_0 S} \tag{13}$$

where l and S are, respectively, the thickness and area of the membrane between the electrodes. Values of the conductivity obtained by the procedure described above are shown at different temperatures in Table 12. The pristine Nafion[®] membrane exhibits higher number moles of water per fixed ionic groups than the hybrid membranes and this circumstance is reflected in a higher conductivity. Neither the size of the fillers nor their sulfonation degree seems to affect the conductivity of the hybrid membranes in a definite way. For example, the NAF-SIL membrane has nearly the same conductivity as the NAF-SEP membrane in spite of the low degree of sulfonation of the fillers in the former membrane at 25ºC and 50ºC, respectively, while the conductivity of NAF-SBA hybrid membranes is about 25% higher for 25ºC and 40% higher at 50ºC. The lowest conductivity observed for NAF-SIL and NAF-SEP membranes reflecting its lowest number of molecules water per fixed group content. However the performance of NAF-SEP membrane at moderate temperatures (80 ºC and 100ºC) is quite similar to NAF-SBA hybrid membrane and pristine Nafion[®] membrane, respectively. It occurs as whether the stronger Nafion-Sepiolite interactions that enhance the glass transition temperature of the molecular chains hinder molecular motions that facilitates the formation of percolation paths through which proton transport occurs.

The conductivity of the membranes NAF, NAF-SIL and NAF-SBA follows Arrhenius behavior in the temperature window 25 – 80º C. However, departure of this behavior is observed at 100º C presumably as a consequence of the loss of humidity in the membrane at this temperature. The activation energies associated with the conductivities obtained from Arrhenius plots in the range 25 – 80ºC are 4.5, 3.9 and 4.8 Kcal/mol, respectively, for the NAF, NAF-SIL and NAF-SBA membranes. These values are slightly higher than those reported for the conductivity of flexible polyelectroytes, such as perfluorosulfonic acid membranes, which amount to 2.4 – 3.6 kcal/mol [48].

4. CONCLUSIONS

Addition of fillers to Nafion[®] slightly reduces the water uptake, though the ion exchange capacity is not significantly affected presumably due to the ionic character of the fillers. Sepiolite presents more favorable interaction with Nafion[®] than the alternative fillers as the enhancement of the glass transition temperature of the Nafion-Sepiolite membrane reflects. In general filler-polymeric matrix interactions result in better mechanical properties. In most cases, fillers slightly decreases oxygen crossover in the membranes. The 10% of fillers content in the hybrid membranes does not produce a severe disruption of the percolation paths through which protons travel across the membranes. In general the conductivity of the hybrid membranes follows the same trends as the water uptake, the Nafion-SBA membrane having similar conductivity as the pristine Nafionâ membrane.

REFERENCES

[1] T. Sata, Ion Exchange Membranes: Preparation, Characterization, Modification and Application. Cambridge: Royal Society of Chemistry, 2004.

[2] Li Qingfeng, He Ronghuan, Jensen J. O. and Bjerrum N. J., Chem. Mater.,15(26), 4896 (2003).

[3] G. Alberti, M. Casciola, Annu. Rev. Mater. Res., 33, 129 (2003).

[4] K. D. Kreuer, J. Membr. Sci., 185, 29 (2001).

[5] S. Yuyan, Y. Geping, W. Zhenbo, G. Yunzhi, J. Power Sources, 167, 235 (2007).

[6] G. Alberti, M. Casciola, Solid State Ionics, 145, 3 (2001).

[7] A. S. Aricò, P. Creti, P. L. Antonucci, V. Antonucci, Electrochem. Solid State Lett., 1, 4 (1998).

[8] Zoppi, R. A, Yoshida I. V. P, Nunes S. P, Hybrids of perfluorosulfonic acid ionomer and silicon oxide by sol-gel reaction from solution: Morphology and thermal analysis. Polymer, 39, 1309 (1998).

[9] G. Alberti, M. Casciola, L. Massinelli, B. Bauer, Journal of Membrane Science, 185, 73 (2001).

[10] B. Bonnet, D. J. Jones, J. Rozière, L. Tchicaya, G. Alberti, M. Casciola, L. Massinelli, B. Bauer, A. Peraio, E. Ramunni, J. New. Mater. Electrochem. Syst., 3, 87 (2000).

[11] Z.-G. Shao, H. Shu, M. Li, I.-M Hsing, Solid State Ionics, 177, 779 (2006).

[12] X. Zhu, H. Zhang, Y. Liang, X. Wang, B. Yi, J. Phys. Chem. B, 110, 14240 (2006).

[13] V. Ramani, H. R. Kunz, J. M. Fenton, J. Memb. Sci., 232, 31 (2004).

[14] U. H. Jung, K. T. Park, E. H. Park, S. H. Kim, J. Power Sources, 159, 529 (2006).

[15] Chalkova E., Pague M. B., Fedkin M. V., Wesolowski D. J., Lvova S. N., J. Electrochem. Soc., 152, A1035 (2005).

[16] E. Chalkova, M. V. Fedkin, S. Komarneni, S. N. Lvov, J. Electrochem. Soc., 154, B288 (2007).

[17] Q. Li, R. He, J. A. Gao, J. O. Jensen, N. J. Bjerrum, J. Electrochem. Soc., 150, A1599 (2003).

[18] A. S. Arico, V. Baglio, A. Di Blasi, V. Antonucci, Electro-

Table 12. Conductivity in S/m for the membranes directly sandwiched between the electrodes as a function of temperature.

T, (ºC)	s, S/m Nafion membrane	s, S/m NAF-SIL membrane	s, S/m NAF-SBA membrane	s, S/m NAF-SEP membrane
25	1.81	1.42	1.86	1.43
50	3.41	2.20	3.79	2.39
80	5.92	3.95	6.03	6.24
100	6.07	4.29	6.38	5.83

Preparation and Characterization of Hybrid Membranes based on Nafion® using Partially Sulfonated Inorganic Fillers
/ J. New Mat. Electrochem. Systems

93

chem. Comm., 5, 862 (2003).

[19]H. L. Tang, M. Pan, J. Phys. Chem. C, 112, 11556 (2008).

[20]Z. G. Shao, P. Hoghee, I.-M. Hsing, J. Membr. Sci., 229, 43 (2006).

[21]F. J. Fernández-Carretero, V. Compañ, E. Riande, J. Power Sources, 173, 68 (2007).

[22]P. L. Antonucci, A. S. Aricò, P. Cretí, E. Ramunni, V. Antonucci, Sol. State Ionics, 125, 431 (1999).

[23]R. F. Silva, S. Passerini, A. Pozio, Electrochim. Acta, 50, 2639 (2005).

[24]S. Aiba, M. Ohashi, S. Huang, Ind. Ing. Chem. Fundam., 7, 497 (1968).

[25]V. Compañ, Mª L. López, A. Andrio, A. López-Alemany, M. F. Refojo, J. of Applied Polymer Sci., 72, 321 (1999).

[26]ISO International Standard 9913-1. Contact Lenses: Part 1: Determination of Oxygen Permeasbility and Transmissibility by the Fatt Method. In International Standards Organization, (ISO) ad. International Standard, Optics and Optical Instruments; Case Postale 56, CH-1211: Geneve, Switzerland, 1996; pp1-13.

[27]V. Compañ; J. Guzmán; E. Riande. membranes Biomaterials, 19, 2139 (1998).

[28]A. Mokrini, M. A. Huneault, J. Power Sources, 154, 51 (2006).

[29]R. Mohr, V. Kudela, J. Schauer, K. Richau, Desalination, 147, 191 (2002).

[30]S. Balci, J. of Chem. Tech. & Biotech., 66, 72 (1996).

[31]J. L. Valentin, M. A. Lopez-Manchado, A. Rodriguez, P. Posadas, L. Ibarra, App. Clay Sci., 36, 245 (2007).

[32]V. Di Noto, R. Gliubizzi, E. Negro, G. Pace, J. Phys. Chem. B, 110, 24972 (2006).

[33]Q. Deng, C. A. Wilkie, R. B. Moore, K. A. Mauritz, Polymer, 39, 5961 (1999).

[34]C. A. Wilkie, J. R. Thomsen, M. L. Mittleman, J. Appl. Pol. Sci., 42, 901 (1991).

[35]S. R. Samms, S. Wasmus, R. F. Savinell, J. Electrochem. Soc., 143, 1498 (1996).

[36]Q. Deng, R. B. Moore, K. A. Mauritz, J. Appl. Pol. Sci, 68, 747 (1998).

[37]G. Socrates. Infrared and Raman characteristic group frequencies: tables and charts. John Wiley & Sons, 2004.

[38]C. del Rio, J. R. Jurado, J. L. Acosta, Polymer, 46, 3975 (2005).

[39]S. de Almeida, Y. Kawano, Journal of Thermal Analysis and Calorimetry, 58, 569 (1999).

[40]I. D. Stefanithis, K. A. Mauritz, Macromolecules, 23, 2397 (1990).

[41]H. R. Corti, F. Nores-Pondal, M. P. Buera, J. Power Sources, 161, 799 (2006).

[42]Ki-Yun Cho, Ho-Young Jung, Kyung A. Sung, Wan-Keun Kim, Shi-Joon Sung, Jung-Ki Park, Jong-Ho Choi, Yung-Eun Sung, J. Power Sources, 159, 524 (2006).

[43]B. Rodmacq, M. Pineri, J. M. D. Coey, A Meagher, J. Polym. Sci. Part B, Polym. Phys., 20, 603 (2003).

[44]Yeo Eisenberg, J. Appl. Polym. Sci., 21, 875 (2003).

[45]K. A. Page, K. M. Cable, R. B. Moore, Macromolecules, 38, 6472 (2005).

[46]J. Brandrup, E. H. Immerqut, E. A. Grulke, Eric A. Grulke, Abe Akihiro, D. Bloch, Polymer Handbook 4th edition: Wiley-Interscience, 1999.

[47]N. G. McCrum, J. Pol. Sci., 34, 355 (1959).

[48]J. Halim, F. N. Büchi, O. Haas, M. Stamm, G. G. Scherer, Electrochim. Acta, 39, 1303 (1994).